Volume 1 | Number 1 | Jan 2013 | Pages 1–100

Journal of
Materials Chemistry A

Materials for energy and sustainability
www.rsc.org/materialsA

Li⁺

ROYAL SOCIETY
OF CHEMISTRY

ROYAL SOCIETY
OF CHEMISTRY

www.rsc.org/materialsA

Journal Name

ARTICLE

Nanostructured p-type Cr/V$_2$O$_5$ thin films with boosted thermoelectric properties

Joana Loureiro,[1] Rafael Santos,[1] Adriana Nogueira,[1] Frederic Wyczisk,[2] Laurent Divay,[2] Sebastian Reparaz,[3] Francesc Alzina,[3] Clivia M. Sotomayor Torres,[3,4] John Cuffe,[5] Fatima Montemor,[6] Rodrigo Martins,[1] and Isabel Ferreira[1]

The urgent need of non-toxic and abundant thermoelectric materials has become a significant motivation to improve the figure of merit of metal oxides in order to remove the barrier towards its widespread use for thermoelectric applications. Here we show the influence of a Cr layer in boosting the thermoelectric properties of Vanadium Pentoxide (V2O5) thin films, deposited by thermal evaporation and annealed at 500ºC. The Cr to V2O5 thickness ratio controls the morphological and thermoelectric properties of the thin films produced. The optimized Seebeck coefficient and Power Factor values are at room temperature +50μV/K and 7.9×10-4 W/mK2, respectively. The nanograin structure of the films is responsible for an improvement in the electrical conductivity up to 3×105(Ω.m)-1 with a typical thermal conductivity of 1.5 W/mK. These results combine to yield promising p-type thermoeletric CrV2O5 thin films with ZT of 0.16 at room temperature.

Keywords: thermoelectrics, thin films, power generation, vanadium pentoxide

1. Introduction

Vanadium oxide thin films have attracted considerable attention as potential candidates for many advanced applications [1] such as: electrochromic devices [2]; thermochromic coatings[3, 4]; metal-semiconductor transition materials [5]; and electrodes for batteries [6]. This diverse range of applications is made possible due to the several stable oxidation states of vanadium oxide (V$_2$O$_5$, VO$_2$, VO, V$_2$O$_3$) which depend on the fabrication process, annealing treatment, and source material [1]. In particular, vanadium pentoxide (V$_2$O$_5$) is characterized by its sheet-like structure due to a distortion of the orthorhombic atoms packing. The electronic transport process above 300 K arises mainly from the hopping of free polarons between vanadium sites that are not associated with oxygen vacancies [7]. Thermoelectric studies on pure V$_2$O$_5$ thin films are scarce in literature. Recently, values of Seebeck coefficient, S = - 218 μV/K, power factor, PF = 2.6×10^{-7} W/K^2 m, and figure of merit, ZT = 1.7×10^{-4} were reported [8] for V$_2$O$_5$ films thinner than 100 nm, which are comparable to those found for thicker V$_2$O$_5$ films of 15 μm [9]. Although the Seebeck coefficient in these studies was relatively large, the PF and ZT still remained small due to the low electrical conductivity, thus rendering the

material unsuitable for any practical thermoelectric applications. Since vanadium oxide is a non-toxic abundant material [10] found in several mineral resources [11] there is a significant motivation to improve its electrical conductivity to obtain large power factors (PF) and better thermoelectric figure of merit (ZT), thus removing the barrier towards its widespread use for thermoelectric applications.

Recently, Density Functional Theory (DFT) simulations [12] have predicted that a controlled doping of V$_2$O$_5$ with metal elements can improve the PF due to a larger electrical conductivity. These results have also been confirmed experimentally, for example, Na alloying has been shown to lead to a significant enhancement of the PF from 10^{-8} W/K^{2}m to 10^{-5} W/K^{2}m [13]. Different vanadium-chromium oxides systems produced by thermal evaporation [14], reactive bias-target ion beam deposition, [15] and chemical synthesis, [16, 17] among others, have been investigated mainly for its good catalytic, [18] electronic and ionic [19] properties, although there has been few studies regarding thermoelectric properties. In this work, a comprehensive study of the influence of morphology on the thermoelectric properties of vanadium oxides thin films doped with Cr is presented relating the nanostructured morphology to record values of PF and ZT. The remarkable increase of PF and

ZT by several orders of magnitude in V_2O_5 films is found, when the films are deposited by thermal evaporation on a very thin Cr layer (< 20 nm) and subsequently annealed at 500 ℃ under atmospheric conditions.

2. Experimental Section

Films Deposition

Thin films of Cr and V_2O_5, in three different thickness proportions (Cr:V_2O_5): 1:1.5, 1:2.5 and 1:3.5, were deposited on Corning glass by the thermal evaporation technique assisted by an electron beam or a resistive crucible. The source materials used were Cr powder with 99% purity (Alfa Aesar GmbH, Germany), and V_2O_5 powder with 99.99 % purity (Super Conductor Materials, Inc., USA). Carbon or tungsten were used for the crucibles. A post-deposition thermal treatment was performed in a furnace (Nabertherm L 3/11/B180) with a controlled temperature ramp up to10 K/min. The samples were annealed for one hour at 773 K in atmospheric conditions [8]. The film thickness was measured with an Ambios XP-200 Profilometer, and in the non-annealed samples the thickness varied between 15 to 20 nm for the Cr layer, and between 30 to 70 nm for V_2O_5 keeping the overall thickness less than 100 nm.

Films characterization

The structural properties of the films were ascertained by X-ray diffraction (XRD) using a PANalytical X'Pert PRO equipped with a X'Celerator detector using Cu$K\alpha$ radiation at 45 kV and 40 mA, in a Bragg-Brentano configuration. XRD difractograms were collected over the angular 2θ range 10–70º, with a scanning step of 0.03° and a total acquisition time of 15 min. The surface microstructure was obtained using a scanning electron microscope with focused ion beam (SEM-FIB) - Zeiss Auriga system, and by an Asylum MFP3D atomic force microscopy (AFM) in non-contact mode with an Olympus AC240TM tip top coated with Al. The Auger Electron Spectroscopy was performed using a PHI 680 Auger Nanoprobe from Physical Electronics, with 3 kV electron beam acceleration. The argon ion energy was 2 keV for sputtering at an average rate of about 4 nm/min. The X-ray photoelectron spectroscopy (XPS) experiments were performed in a Microlab 310 (Thermo Electron – former VG Scientific) system equipped with a non-monochromated Mg anode and a concentric hemispherical analyzer. The XPS spectra were taken in CAE mode (20 eV), using an non-monochromate Al anode. The accelerating voltage was 15 kV. The quantitative XPS spectra were fitted using a Gaussian-Lorentzian product function and an algorithm based on the Simplex optimisation as used in the Avantage software. The binding energies assigned to the different species were determined from peak fitting. The deviations assumed in the fitting procedures for the chemical identification, were ± 0.1 eV. The background was subtracted using the Shirley algorithm assuming the intensity of the

background proportional to the peak area on the higher kinetic energy side of the spectra.

Thermoelectric properties

The thermal conductivity of the samples was measured using the time-domain thermoreflectance (TDTR) technique, as discussed in Refs. [20, 21]. An Al layer with a thickness of 93 +/- 3 nm was deposited by electron beam evaporation to act as a transducer layer. A pump laser pulse with a pulse duration of 200 fs and wavelength of 400 nm was used to heat the sample, causing a temperature-dependent change in reflectivity. This transient reflectivity was recorded over time by a series of 800 nm probe pulses and related to the surface temperature via the thermoreflectance coefficient. The observed cooling curve was then fit to a 3 layer multidimensional model, including the Al transducer, an effective CrV_2O_5 layer, the glass substrate and appropriate thermal interface resistances. This model is based on the Fourier model of heat conduction model and as such does not account for potential non-diffusive effects over short lengthscales [20]. The measured thermal conductivity can therefore be considered as an effective value considering diffusive transport. A sensitivity analysis was performed to ensure that the fitting model was sensitive to the thermal conductivity values of the CrV_2O_5 layer within experimental uncertainty [21]. The measurements were averaged over three sample locations, with multiple traces taken for each location. The pump pulses had a repetition rate of 80 MHz and were modulated with frequencies ranging from 3 – 12 MHz for lock-in detection. The electrical conductivity was calculated from the linear I-V plot obtained by a Cascade Microtech/Alessi REL-4500 probing platform connected to a HP 4145B Semiconductor Parameter Analyzer. The carriers Hall mobility (μ) and concentration (N) were measured through a Hall-effect measurement system (Bio Rad HL 5500) using the van der Pauw configuration. The Seebeck coefficient ($S=\Delta V/\Delta T$) values were obtained by measuring the thermovoltage ΔV as a function of the temperature gradient ΔT, keeping the average temperature constant at 293 K. For that 1 mm × 4 mm Al contacts 2 mm apart, were deposited on the film and the samples were placed between two TEC1-12707 Peltier modules with each connected to a power source so that one can be turned hot and the other cold. The temperature gradient created in the plane over the 2 mm length was continuously monitored with a FLIR A310 thermal camera equipped with a macro lens having a sensitivity of 50 mK. The thermovoltage was measured using a nanovoltmeter (Agilent 34420A). For the I-V measurements, a variable load resistance was connected in series with the thermoelectric element and the thermovoltage was monitored as a function of the total resistance, for three temperature gradients (2.5, 4.5 and 7.5 K).

3. Results

In the next sections a detailed analysis is presented showing the influence of the Cr to V_2O_5 ratio on the morphology,

composition, electrical, thermal, and thermoelectric properties of the Cr/V_2O_5 thin films.

3.1. Structure Morphology and Composition

The XRD patterns in Figure 1 show the influence of the $Cr:V_2O_5$ ratio on the crystallinity of the dual layer structure after annealing. The typical orthorhombic V_2O_5 structure (PDF card no. 00-041-1426) [22] and that of cubic Cr (PDF card no. 00-006-0694) [22] are displayed to help the identification of the peaks. All diffractograms of the V_2O_5 films show a preferential orientation along (001) ascribed to the $2\theta=20°$ peak. A small peak corresponding to the cubic Cr is also visible and as the V_2O_5 to Cr ratio increases, the (001) peak intensity increases and growth along other planes: {00h}, {0h0} and {011} takes place. The crystallite grain size for the three different films was estimated by the Scherrer's formula [23] and corresponds to 13.5, 28.3 and 24.3 nm, for the 1:1.5, 1:2.5 and 1:3.5 ratios, respectively. The broad bump observed around 22° is due to the glass substrate.

The surface morphology of the studied films is shown in Figure 2. The SEM surface images (a, b and c) shows crystallized films with different grain sizes. The preferred growth direction is perpendicular to the plane of the substrate which is consistent with the orientations obtained by XRD. All films have large grain domains of approximately 100 nm lateral size, which are in turn made up of small grains (1:1.5) or sheet-like grains (1:2.5, 1:3.5). The average root mean square (RMS) roughness is between 3-6 nm for all films. The AFM phase images (d, e, f) emphasize the variation of the phase along the analyzed sample area. A slight phase change is observed for the 1:1.5 samples while the other samples have a phase variation of nearly 60°. In general this can be correlated to regions of the samples with voids or changes in material. Here, we attribute the differences in phase to voids between grain domains boundaries, since according to the SEM images and to the Energy Dispersive Spectrometry (EDS) mapping obtained (not shown), there are no Cr or V_2O_5 segregation regions.

During the deposition of the V_2O_5 layer on the previously deposit Cr layer, a thin interdiffusion layer (< 1 nm) may be formed. However, the thermal annealing promotes the interdiffusion of atoms and a thicker intermediate Cr/V_2O_5 layer is formed. In order to determine the extent of Cr penetration into V_2O_5 layer, AES depth profiles were obtained for the three different Cr/V_2O_5 ratios as shown in Figure 3. The data confirms the diffusion of Cr into the V_2O_5 layer.

Moreover, the two Cr peaks depicted with dash lines shows the existence of two phases, one corresponding to Cr-Cr bonds (due to the presence of Cr still in its metallic phase) and another one corresponding to Cr-O (either from simple Cr_xO_y or from V_2O_5 doping, $Cr_xV_yO_z$). The Cr diffusion length into the V_2O_5 was found to be the same for the three thicknesses ratios, namely ~ 30 nm (considering the 4.2 nm/min etch rate), since the same annealing temperature and procedure were used with all samples, therefore the overall structure is similar.
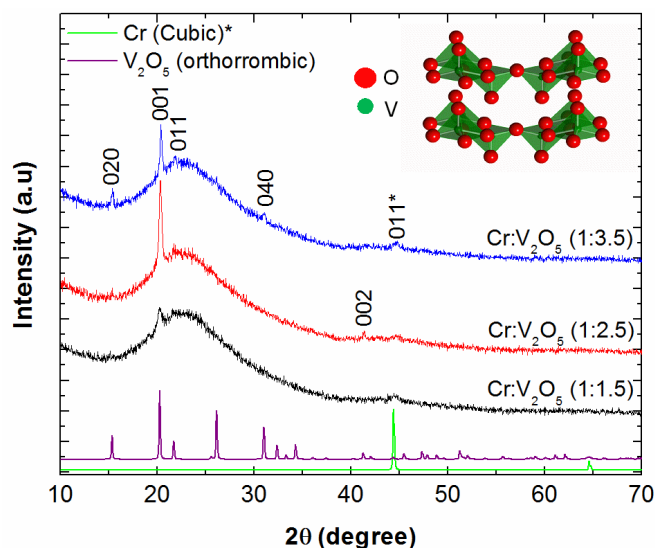

Fig. 1: The XRD diffractograms of the films with three different $Cr:V_2O_5$ thickness ratios are here depicted, together with the V_2O_5 (PDF 00-041-1426) and Cr powders (PDF 00-006-0694) diffractograms for comparison. The inset shows the typical orthorhombic structure of V_2O_5 which is kept for the three ratios.
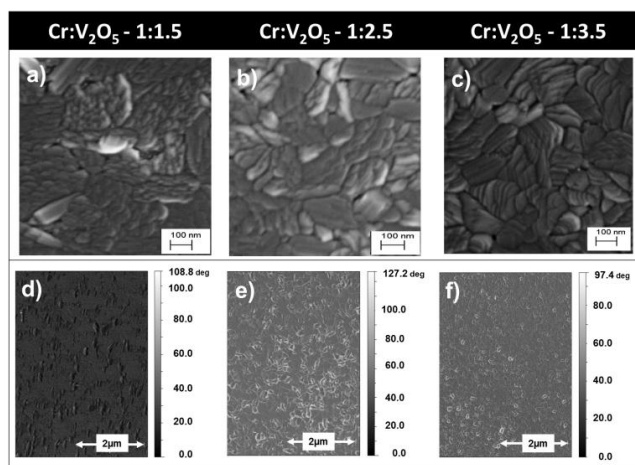

Fig. 2: SEM photos (a, b, c) and AFM phase variation images (d, e, f) for the three $Cr:V_2O_5$ ratio films.

The Cr diffusion into the V_2O_5 layer is expected to strongly influence both the electrical and thermal conductivity properties of films.

Complementary XPS data are shown in Figure 4 with the ionization peaks for Cr2p3/2 and V2p3/2 before and after annealing the $Cr:V_2O_5$ (1:2.5) film. Before annealing, the Cr2p3/2 ionization spectrum shows a peak with low intensity at approximately 574.0 eV, which can be assigned to metallic Cr and a shoulder at higher binding energies that can be attributed to Cr^{3+} species (577.4 eV). After annealing, the main peak appears at higher binding energy, whereas the one at lower energies vanishes. This indicated that Cr becomes more oxidized and most probably appears in a non-stoichiometric form like Cr_xO_y (y>x) therefore with a valence C^{+b}, b≥+3. The

peak corresponding to metallic Cr (~574 eV) shifts towards higher values, (577.6 eV), which is in agreement with the Auger profile where the Cr oxidation shifts the metallic Cr peak towards lower values in kinetic energy. Therefore, Cr in its metallic form should be present near the substrate and Cr_xO_y or $Cr_xV_yO_z$ in the interface between Cr and V_2O_5. Concerning the vanadium valence, a shift towards higher energy values (~516.8 eV) is also visible, corresponding to oxygen enrichment with the dominant valence being V^{5+} (V_2O_5 phase) after annealing which is responsible for a degenerated semiconductor-like behavior.

3.2. Electrical and Thermoelectric Properties

The in-plane electrical conductivity of the films was measured with top contacts on the V_2O_5 thin films. As shown in table 1 the conductivity increased more than five orders of magnitude compared to that of the V_2O_5 single layer [8] for all the studied Cr/V_2O_5 ratios (table 1). The large increase in the electrical conductivity is mostly attributed to the increased majority carrier concentration (N). Independent of the presence of Cr the electron mean free path is basically determined by the grain size. Typically, for non-intentionally doped crystalline V_2O_5 thin films N is of the order of 10^{15} cm^{-3}, and electrical transport is dominated by n-type carriers [8], whereas in the Cr/V_2O_5 layers it increases up to 10^{21} cm^{-3}, corresponding to an increase of six orders of magnitude, and the electrical transport is dominated by p-type carriers.

The hall mobility (μ) for the holes is calculated from $N=\sigma/(q.\mu)$, where σ is the electrical conductivity, q the electron charge and μ the mobility of the carriers. The hole mobility for each thin film is shown in table 1. The measured mobility values are around 4 cm^2/Vs, except for the sample with the highest V_2O_5 to Cr ratio. These values are two orders of magnitude higher than those found in literature for amorphous chromium oxide and even higher compared to crystalline CrO_2 or Cr_2O_3 crystalline oxides. [24] For comparison, table 1 also shows the properties of a 10 nm thick Cr layer. The mobility values are much lower than those found in literature for pure Cr, as shown in Table 1. However, since the measurements were performed at atmospheric pressure, the formation of Cr native oxides is expected and may influence the measure values. The V_2O_5 layers were deposited in this Cr layer, after being exposed to atmospheric pressure since the process includes a vacuum break. It is important to note that Cr and Cr/V_2O_5 were measured in similar experimental conditions. The measurements of conductivity versus temperature revealed that films have very small or non-detectable thermal activation energy but the optical gap is preserved in 2.7-2.8 eV as reported for V_2O_5 [8] therefore, they behave as degenerated semiconductors, similar to Transparent Conductive Oxides (TCO) materials. The transmittance of Cr/V_2O_5 has decreased in comparison to the single V_2O_5 layer[8] and depending on the thickness of Cr it is between 30 and 50%. The thermoelectric voltage (ΔV) as a function of temperature gradient (ΔT) has

been measured and the linear dependence observed had a positive slope (positive Seebeck coefficient, S) which confirms that the majority carriers are p-type.
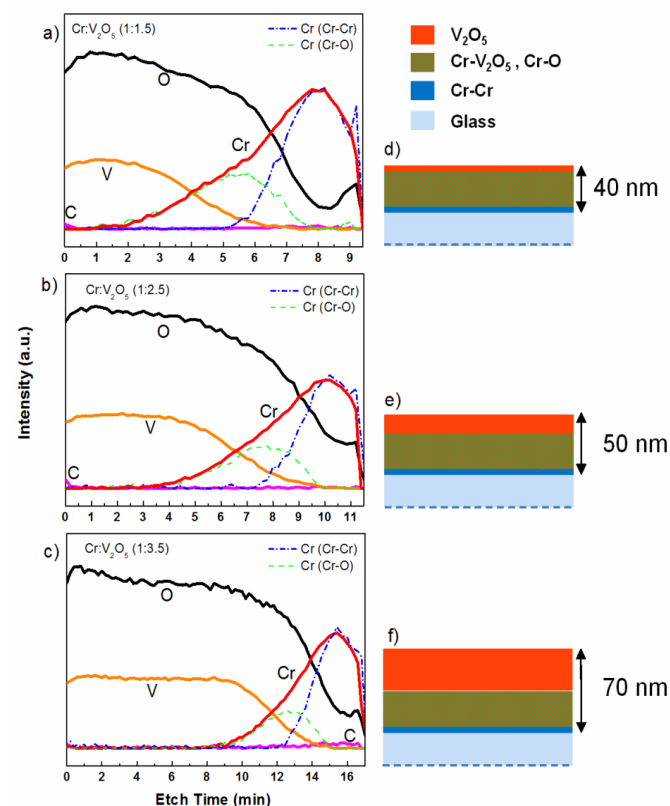

Fig. 3: AES spectra for samples with a ratio of 1:1.5 (a), 1:2.5 (b) and 1:3.5 (c) after annealing at 500ºC. . The total Cr presence (red) is the combination of the metallic Cr-Cr phase (blue dash-dot) near the substrate and oxide Cr-O phase (green dash) within the interdiffusion region. The presence of vanadium and oxide is represented in orange and black respectively. The presence of C is due to contamination. The etch rate was about 4 nm.min^{-1}.

Although the highest S values were obtained for a Cr/V_2O_5 ratio of 1:2.5, the electrical conductivity is much higher for films produced with a $Cr:V_2O_5$ ratio of 1:1.5, leading to an optimized power factor (PF = σS^2) of 1.0×10^{-3} W/K^{2}m, as shown in table 1.

The power factor of the $Cr:V_2O_5$ multilayers are improved up to four orders of magnitude as compared to V_2O_5, mainly due to the improvement of the electrical conductivity. However, compared to the properties of the Cr single layer, the thermal conductivity in Cr/V_2O_5 is much lower as thin metal films typically have larger thermal conductivity than oxides. [25]

Concerning the influence of Cr to V_2O_5 ratios on the thermal conductivity (k), the results show that the sample with the 1:1.5 thickness ratio has the highest k in accordance with its large Cr content. It was not possible to measure the thermal conductivity accurately in this sample due to low experimental sensitivity for high k values.

Journal Name

ARTICLE

Table 1: Room temperature electrical and thermoelectrical properties of the films obtained with different $Cr:V_2O_5$ ratios. The * denotes calculated using the Wiedemann–Franz law (see text). SC means semiconductor type.

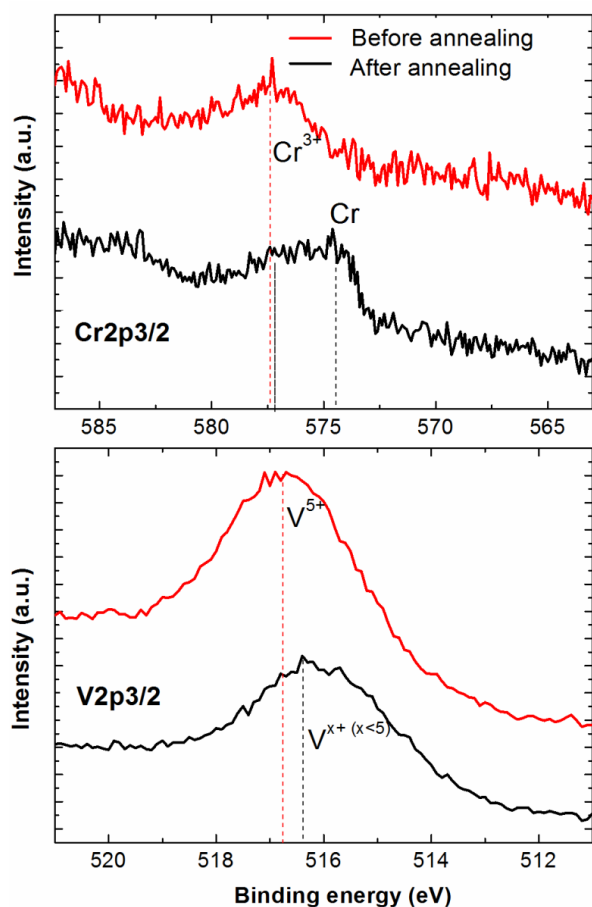| $Cr:V_2O_5$ ratio	S ($\mu V/K$)	σ ($\Omega.m$)$^{-1}$	μ (cm^2/Vs)	N (cm^{-3})	PF (W/K^2m)	k (W/mK)	$k_{el\text{-}WF}$* (W/mK)	ZT	SC Type
1:1.5	41.1±2.1	6.0×10^5	3.9	9.6×10^{21}	1.0×10^{-3}	>5	4.39	<0.06	P
1:2.5	50.3±0.6	3.1×10^5	4.0	4.9×10^{21}	7.9×10^{-4}	1.47	2.27	0.16	P
1:3.5	36.7±0.6	1.5×10^5	1.4	6.7×10^{21}	2.0×10^{-4}	1.54	1.1	0.04	P
Cr	35.7±0.4	1.67×10^6	0.6	1.6×10^{23}	2.1×10^{-3}	-	12.2	<0.05	P
V_2O_5 (annealed) [8]	-218	5.5	-	10^{15}	2.6×10^{-7}	0.45	4×10^{-5}	2×10^{-4}	N

Fig. 4: XPS of a Cr/V_2O_5 sample with a ratio of 1:2.5 showing the ionization peaks for Cr2p3/2 and V2p3/2 before (black) and after (red) annealing.

However, if we attribute the large thermal conductivity to the charge carriers introduced by Cr doping, a crude estimate of the thermal conductivity can made from the Wiedemann–Franz (WF) law $k_{el\text{-}WF} = \sigma LT$, where σ is the electrical conductivity, L is the Lorentz number for metals (L = 2.44×10^{-8} $W.\Omega.K^{-2}$) and T is the temperature, as shown in table 1. Even though this sample shows good electrical performance, the large thermal conductivity of ~ 5 W/m/K results in a relatively low value of ZT = 0.06. The largest figure of merit ZT = 0.16 is obtained in the thin films with a 1:2.5 $Cr:V_2O_5$ ratio, which exhibits simultaneously a low thermal conductivity and high power factor. Interestingly, for these films, the total k is lower than the $k_{el\text{-}WF}$ suggesting that WF law is inadequate, and resulting in an effective Lorentz number of $1.6x10^8$. This is because the Lorentz number of a degenerate semiconductor depends heavily on both doping and dimensionality, and has been observed to decrease for thin thermoelectric films. [26-28]

The output voltage and power of the films with the highest ZT were measured and are shown in Figure 5. The current–voltage characteristic of the thermoelectric element is expected to be linear, as described by the equation $V_{out}=S\Delta T-IR_{int}$ where V_{out} is the output voltage, I is the current flowing on the circuit with the different load resistances and R_{int} is the 4 mm x 2 mm thermoelectric element resistance (the contacts resistances are negligible when compared to the thermoelectric element resistance). The output power (P_{out}) is described by the equation $P_{out}=S\Delta TI-I^2R_{int}$. The voltage and power outputs obtained for the highest temperature gradient applied, 7.5 K, are described by the equations: $V_{out}=3.14\times10^{-4}$ - 23.1 I and $P_{out}=3.85\times10^{-4}$ I – 29.8 I^2, respectively, in good agreement with the classical theoretical models [29], also represented in figure 5.

The thermoelectric element has its maximum power output when the load resistance is equal to the inner resistance R_{int} and the current at the point of maximum power is half of the short circuit current. In this case, the maximum power of the thermoelectric element, at a certain temperature difference, is
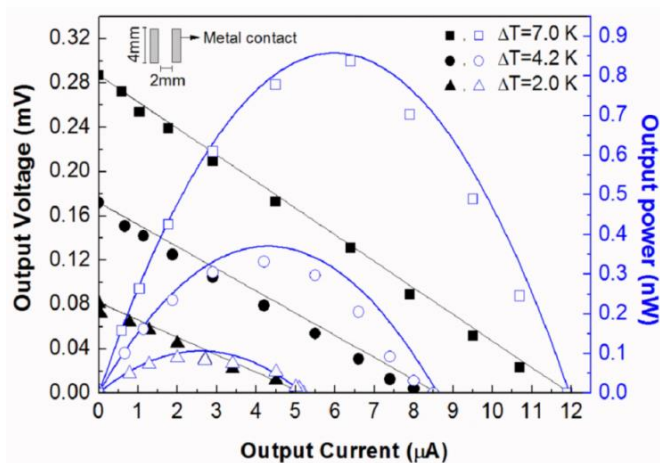
Fig. 5: Output voltage (solid symbols) and output power (open symbols) versus current for samples produced with a Cr:V_2O_5 ratio of 1:1.5 for three temperature gradients: 2.0 K (triangles), 4.2 K (circles) and 7.0 K (squares). Solid lines represent the theoretical curves and the solid elements represent the experimental data.

$P_{max} = S^2 \Delta T^2 / 4R_{int}$.[29] For the three ΔT measurements, the P_{max}, I_{Pmax} and V_{Pmax} are shown in table 2.

Based on the parameters trend it was possible to estimate a maximum power output of 8.4 nW for $\Delta T = 20$ K (together with the output voltage and current in that situation, as shown in table 2). It is important to emphasize that these results were obtained for a single p-type TE element. Although this power output power is small for most applications, it is already comparable to full devices comprising 100 thin film thermocouples of Sb_2Te_3/Bi_2Te_3, also working with in plane geometry, that for $\Delta T = 20$ K have a maximum power output of 7 nW.[30] By connecting this p-type thermoelectric element with a compatible n-type element and playing with series and parallel interconnections between the thermocouples it will be possible to design devices with higher output powers (focusing low power applications).

Table 2: For each temperature gradient the maximum values of Power, Voltage and Current are depicted, with * denoting simulated values.

ΔT	P_{max} (nW)	I_{Pmax} (μA)	V_{Pmax} (mV)
2.0	0.10	2.29	0.045
4.2	0.37	4.30	0.086
7	0.85	6.52	0.130
20	8.4*	20.5*	0.410*

3.3. Discussion

The overall analysis of these results clearly show a significant enhancement of the thermoelectric properties of V_2O_5 films deposited over a Cr layer. The largest value of ZT = 0.16 was achieved for Cr:V_2O_5 layers with a total thickness of 50 nm in a ratio of 1:2.5.

According to our previous results, [8] the as-deposited V_2O_5 amorphous films crystallize in a orthorhombic structure after annealing at 500 ºC during 1h under atmospheric pressure. As predicted by Chumakov et al. [12] the doping of V_2O_5 with metal elements ($M_xV_2O_5$) can increase the electrical conductivity of the films by more than three orders of magnitude and the semiconductor character of the V_2O_5 changes to a metallic-like behavior. Indeed we have experimentally verified that the activation energy of CrV_2O_5 films is very small ($<10^{-2}$ eV). Again, as previously predicted[12] the Seebeck coefficient decreased by a factor of five with metal doping, however, experimentally we found in-plane anisotropy of both the Seebeck coefficient and electrical conductivity. Furthermore, according to the SEM images the films are formed by grains with domains constituted by several stacked layers. These grains are larger for higher Cr:V_2O_5 ratios (increasing from 13.5 nm up to 28.3 nm) and the AFM phase analysis also reveals that for lower ratios this phase is constant along the 2 μm^2 area analyzed. The variation of the phase may be related to voids at grain boundaries and these will contribute to trap free carriers, reducing the electrical conductivity. This is in agreement with the obtained results for the electrical conductivity, which was smaller for the larger ratios (1:2.5 and 1:3.5). As observed by other authors, the decrease in grain sizes also benefits the thermoelectric properties due to potential barrier scattering at grains boundaries [31, 32] which may explain why the films produced at the highest Cr:V_2O_5 ratio have lower Seebeck coefficient values.

We note that although the parameters (S, σ, and k) used to calculate the power factor must be measured in the same crystallographic orientation, in the present experiments the thermal conductivity is measured in the cross-plane direction, whereas the other quantities are obtained in the in-plane orientation. However, since phonon scattering is thought to be mostly dominated by grain boundaries the cross plane thermal conductivity is expected to be equivalent to the in-plane conductivity allowing for a consistent calculation of ZT.

We also note that the majority carriers in the V_2O_5 changed from n-type to p-type when deposited on the Cr layers. To date, no p-type thermoelectric $Cr_xV_yO_z$ alloys have been demonstrated and trials to obtain p-type metal oxides from $d^{10}s^2$ cations have been unsuccessful due to the two closed shells. However, using $d^{10}s^1$ cations introduces a covalence in the metal–oxygen bonding which induces the formation of an extended valence-band structure. If the energy level of the uppermost closed shell of the metallic cation (in this case of the Cr) is almost equivalent to those of the 2p levels of the oxide ions, the resultant hybridization can delocalize any holes of the valence band, improving the conductivity and a p-type conductive oxide is achieved [33, 34]. This is in good agreement with the observation reported here. Since the 3d shell of chromium has an unclosed configuration it favors d-d transitions and p-type conduction although the transparency of the Cr/V_2O_5 films is inferior to other p-type TCOs.

4. Conclusion

In conclusion, vanadium pentoxide films deposited by thermal evaporation on very thin Cr layers have shown high electrical conductivity and high power factor at room temperature with properties dependent on the $Cr:V_2O_5$ ratio. The best PF result was obtained for a ratio of 1:1.5, with a Seebeck coefficient of $+41.1 \mu V/K$ and an electrical conductivity of 2.5×10^5 $(\Omega.cm)^{-1}$ leading to a maximum power factor of 4.3×10^{-4} $W/K^2 m$. However, the high thermal conductivity of this sample led to a low value of ZT < 0.06. On the other hand, for the 1:1.25 ratio sample, the low measured thermal conductivity of ~ 1.5 (W/mK) combined with a large PF of 7.9×10^{-4} led to a ZT = 0.16, which is the highest obtained for a V_2O_5 alloy to date. We demonstrated that at the maximum output power at room temperature of one element is expected to be 2.5 nW for a temperature gradient of 20 K. The integration of this element with a similar n-type element will comprise a competitive thermoelectric couple for planar flexible thin film thermoelectric devices, with a broad range of low power applications. These results demonstrate the potential of engineering low cost, abundant materials for efficient thermoelectric operation at moderate temperatures between 300 and 400 K.

Acknowledgements

Notes

[1]CENIMAT/I3N-CEMOP/UNINOVA, Faculdade de Ciências e Tecnologia Universidade Nova de Lisboa, 2829-516, Portugal, E-mail: joa.loureiro@gmail.com

[2]Thales Research and Technology, Palaiseau Cedex, 91767, France

[3]Catalan Institute of Nanoscience and Nanotechnology ICN2, Campus UAB, Edifici ICN2, 08193 Bellaterra (Barcelona),Spain

[4]Catalan Institution for Research and Advanced Studies, 08010 Barcelona, Spain

[5]Department of Mechanical Engineering, Massachusetts Institute of Technology, Cambridge, MA 02139, USA

[6]Instituto Superior Técnico, Universidade Técnica de Lisboa, ICEMS, Av. Rovisco Pais, 1049-001 Lisboa, Portugal

References

1. S. Beke, *Thin Solid Films*, 2011, **519**, 1761-1771.
2. C. G. Granqvist, P. C. Lansåker, N. R. Mlyuka, G. A. Niklasson and E. Avendaño, *Solar Energy Materials and Solar Cells*, 2009, **93**, 2032-2039.
3. A. Ilinski, F. Silva-Andrade, E. Shadrin and V. Klimov, *Journal of Non-Crystalline Solids*, 2004, **338-340**, 266-268.
4. F. B. Dejene and R. O. Ocaya, *Current Applied Physics*, 2010, **10**, 508-512.
5. T. Driscoll, H. T. Kim, B. G. Chae, M. Di Ventra and D. N. Basov, *Applied Physics Letters*, 2009, **95**, 043503 - 043503-043503.
6. D. Munozrojas and E. Baudrin, *Solid State Ionics*, 2007, **178**, 1268-1273.
7. C. Sanchez, M. Henry, J. C. Grenet and J. Livage, *Journal of Physics C: Solid State Physics*, 1982, **15**, 7133-7141.
8. R. Santos, J. Loureiro, A. Nogueira, E.Elangovan, J.V.Pinto, J.P.Veiga, T. Busani, E.Fortunato, R.Martins and I.Ferreira, *Applied Surface Science*, 2013.
9. E. Lazaro, M. Bhamidipati, M. Aldissi and B. Dixon, *Thermoelectric Organics*, 1998.
10. Paz Vaqueiro and A. V. Powell, *J. Mater. Chem.*, 2010, **20**, 9577-9584.
11. R.R. Moskalyk and A. M. Alfantazi, *Minerals Engineering*, 2003, **16** 793-805.
12. Y. Chumakov, S. Y. Xiong, J. R. Santos, I. Ferreira, K. Termentzidis, A. Pokropivny, P. Cortona and S. Volz, *Journal of Electronic Materials*, 2012.
13. S. Iwanaga, M. Marciniak, R. B. Darling and F. S. Ohuchi, *Journal of Applied Physics*, 2007, **101**, 123709 - 123709-123708.
14. A. Maetaki, M. Yamamoto, H. Matsumoto and K. Kishi, *Surface Science*, 2000, **445** 8.
15. J. L. Kevin G.West , Li He, David Kirkwood, Wei Chen, T. Paul Adl, Michael S. Osofsky, Syed B. Qadri, Robert Hull,Stuart A.Wolf, *Journal of Superconductivity and Novel Magnetism*, 2008, **21**, 87-92.
16. O. Pozdnyakova, J. Megyeri, E. Kuzmann and L. Szirtes, *Central European Journal of Chemistry*, 2008, **4**, 760-766.
17. O. Pozdnyakovaa, E. Kuzmannb and L. Szirtesa, *Solid State Ionics*, 2003, **161** 301-307.
18. C. M. Pradier, F. Rodrigues, P. Marcus, M. V. Landau, M. L. Kaliya, A. Gutman and M. Herskowitz, *Applied Catalysis B: Environmental* 2000, **27**, 73-85.
19. P. Soudan, J. P. Pereira-Ramos, J. Farcy, G. Grégoire and N. Baffier, *Solid State Ionics*, 2000, **135**, 291-295.
20. A. J. Minnich, G. Chen, S. Mansoor and B. S. Yilbas, *Physical Review B*, 2011, **84**, 235207 - 235207-235208.
21. A. J. Schmidt, X. Chen and G. Chen, *Review of Scientific Instruments*, 2008, **79**, 114902 - 114902-114911.
22. *Joint Committee on Powder Diffraction Standards - International Centre for Diffraction Data*, 2001.
23. V. Melnik, I. Khatsevych, V. Kladko, A. Kuchuk, V. Nikirin and B. Romanyuk, *Materials Letters*, 2012, **68**, 215-217.
24. P. Qin, G. Fang, N. Sun, X. Fan, Q. Zheng, F. Chen, J. Wan and X. Zhao, *Thin Solid Films*, 2011, **519**, 4334-4341.
25. T. M. Tritt, *Thermal Conductivity: Theory, Properties and Applications*, Springer, 2004.
26. P.-O. Chapuis, M. Prunilla, A. Shchepetov, L. Schneider, S. Laakso, J. Ahopelto and C. M. Sotomayor Torres, *16th International Workshop on Thermal Investigations of ICs and Systems (THERMINIC)*, 2010, 1 - 6.
27. A. J. Minnich, M. S. Dresselhaus, Z. F. Ren and G. Chen, *Energy & Environmental Science*, 2009, **2**, 466.
28. R. Venkatasubramanian, E. Siivola, T. Colpitts and B. O'Quinn, *Nature*, 2001, **413**, 597-602.
29. I. Sateikis, R. Ambrulevicius and S. Lynikiene, *Electronics & Electrical Engineering*, 2010, **10**, 113-116.
30. L. Francioso, C. De Pascali, I. Farella, C. Martucci, Creti, x., P., P. Siciliano and A. Perrone, *Sensors*, 2010 IEEE, 2010.
31. K. Kishimoto and T. Koyanagi, *Journal of Applied Physics*, 2002, **92**, 2544.
32. C.-H. Kuo, H.-S. Chien, C.-S. Hwang, Y.-W. Chou, M.-S. Jeng and M. Yoshimura, *Materials Transactions*, 2011, **52**, 795-801.
33. H. Kawazoe, H. Yanagi, K. Ueda and H. Hosono, *MRS Bulletin*, 2000, **25**, 28-36.
34. J. Tate, M. K. Jayaraj, A. D. Draeseke, T. Ulbrich, A. W. Sleight, K. A. Vanaja, R. Nagarajan, J. F. Wager and R. L. Hoffman, *Thin Solid Films*, 2002, **411**, 119-124.